The University of
Nottingham

UNITED KINGDOM · CHINA · MALAYSIA

Bartlett, Philip N. and Burt, Jennifer and Cook, David A. and Cummings, Charles Y. and George, Michael W. and Hector, Andrew L. and Hasan, Mahboba M. and Ke, Jie and Levason, William and Pugh, David and Reid, Gillian and Richardson, Peter W. and Smith, David C. and Spencer, Joe and Zhang, Wenjian (2016) A versatile electrolyte system for electrodeposition of p-block elements from single ohase supercritical CH2F2. Chemistry - a European Journal, 22 (1). pp. 302-309. ISSN 1521-3765

# A Versatile Electrolyte System for Electrodeposition of p-Block Elements from Single Phase Supercritical CH$_2$F$_2$

Philip N. Bartlett,[a]* Jennifer Burt,[a] David A. Cook,[a] Charles Y. Cummings,[a] Michael W. George,[b] Andrew L. Hector,[a] Mahboba M. Hasan,[a] Jie Ke,[b] William Levason,[a] David Pugh,[a] Gillian Reid,[a] Peter W. Richardson,[a] David C. Smith,[b] Joe Spencer,[b] Wenjian Zhang[a]

[a] *Chemistry, University of Southampton, Highfield, Southampton SO17 1BJ, UK.*

[b] *Department of Chemistry, University of Nottingham, University Park, Nottingham NG7 2RD, UK.*

[c] *Physics and Astronomy, University of Southampton, Highfield, Southampton SO17 1BJ, UK.*

ABSTRACT: We describe a electrolyte bath that can be used to electrodeposit a range of p-block elements from supercritical difluoromethane (sc-CH$_2$F$_2$). The bath comprises the tetrabutylammonium chlorometallate complex of the element in an electrolyte of $50 \times 10^{-3}$ mol dm$^{-3}$ tetrabutylammonium chloride at 17.2 MPa and 358 K. Using the anionic ([GaCl$_4$]$^-$, [InCl$_4$]$^-$, [GeCl$_3$]$^-$, [SnCl$_3$]$^-$, [SbCl$_4$]$^-$, and [BiCl$_4$]$^-$) and dianionic ([SeCl$_6$]$^{2-}$ and [TeCl$_6$]$^{2-}$) chlorometallate complexes we demonstrate the deposition of elemental Ga, In, Ge, Sn, Sb, Bi, Se, Te.  In all cases, with the exception of Ga which is a liquid under the deposition conditions, the resulting deposits are characterised by scanning electron microscopy, energy dispersive X-ray analysis, X-ray diffraction and Raman. An advantage of this electrolyte system is that the reagents are all crystalline solids that are reasonably easy to handle and that are not highly water or oxygen sensitive. The results presented here significantly broaden the range of materials accessible by electrodeposition from supercritical fluid and open the future possibility to deposit binary or ternary alloys and compounds of the p-block.

**INTRODUCTION**

---

* Corresponding author.  E-mail: p.n.bartlett@soton.ac.uk

The technology of electroplating (or electrodeposition) of metals arose quite rapidly in the 19th century following the invention of the voltaic pile by Alessandro Volta in 1800. Thus in 1805 Luigi Brugnatelli described the electrodeposition of gold onto a silver medal in a letter to Baptiste von Mons[1] and by 1839 scientists in Britain and Russia had independently devised a process for copper plating. The first viable patents for the electroplating of gold and silver were issued to Henry and George Elkington from Birmingham, UK in 1840 and from there the technology spread rapidly in Europe and then America.

As a materials deposition technology electrodeposition has a number of key features that distinguish it. Electrodeposition is an additive process where the deposition is spatially localised to the electrode surface and occurs directionally away from that surface. As a consequence, the method can be used for conformal deposition onto complex, three dimensional, shapes – as in the case of Brugnatelli's deposition onto a silver medal. In addition, the method has the ability to fill volume without shrinkage and is very efficient in its use of material. Finally, the process is controlled by the applied potential or current and so can be stopped and started at will, and can be directly monitored during the operation. Many of these features distinguish electrodeposition from other widely used materials' deposition technologies such as physical vapour deposition, chemical vapour deposition, atomic layer deposition, or molecular beam epitaxy.

Despite these distinguishing features electrodeposition is often perceived as a "low tech" deposition method only suitable for protective or decorative finishes where purity of the deposit is less important. The perception that electrodeposited material is necessarily less pure that from other deposition routes is unfounded. For example Schindler and Kirschner [2] have shown that it is possible to prepare clean epitaxial magnetic films by electrodeposition of a quality equal to those prepared by molecular beam epitaxy even for fairly reactive materials. There are a number of fundamental reasons why this is true[2]. Firstly, purification of the reagents, electrolytes and solvent reduces the exposure rate, given the typical concentrations and mass transport rates in solution, to $10^{-3}$ ML s$^{-1}$, comparable to the situation in UHV at 5 x $10^{-9}$ mbar assuming unity sticking probability. However, for electrodeposition the situation is rather different because the sticking probability for contaminants is generally much less than unity reducing the exposure rate to $10^{-4}$ ML s$^{-1}$, comparable to 5 x $10^{-10}$ mbar in UHV. In addition, for electrodeposition the dense medium opens up the possibility of using high concentrations of species to stabilise the growing surface against unwanted side reactions, for example by cation adsorption.

Further evidence of the abilities of electrodeposition to contribute to the deposition of high quality materials in critical applications can be found in the copper Damascene process pioneered by IBM and used to deposit electrical interconnects on VLSI silicon chips. [3] The commercial adoption of this process to replace aluminium interconnects by copper in integrated circuits has been essential to the progress of VLSI to its current level.

In electrodeposition the electrolyte (that is the combination of solvent and dissolved ions) plays a key role in determining what can be deposited. The majority of electrodeposition, from the Damascene copper process used in VLSI manufacture to the deposition of copper vias on PCB boards and the electrodeposition of magnetic materials in read-write heads,[4] uses aqueous solutions. However, water severely limits the range of materials which can be deposited. This is, at least in part, because water can react as an acid or base and because it is easily oxidised or reduced (the accessible electrochemical potential window is around 1.3 V). These restrictions can be overcome by using non-aqueous solvents or ionic liquids. Ionic liquids have been used in electrochemistry and electrodeposition since the 1980s. [5,6] They offer flexibility in the choice of solvent properties and a wide electrochemical window. As a result there is considerable activity worldwide in electrodeposition from ionic liquids and a range of materials (including Cr, Mn, Ni, Sn, Cu, Ag, Co, Si and Ge) have been deposited with different degrees of success. However, significant challenges remain to achieve device quality semiconductor materials and the high viscosity and surface tension of ionic liquids means they are poorly suited to electrodeposition into extreme (sub 20 nm) nanostructures.

The desire for faster and more powerful semiconductor devices continues to drive materials' deposition to smaller and smaller scales; here the interest in nanotechnologies and the investigation of "bottom up", as opposed to the conventional "top-down", approaches to device fabrication. Many conventional material deposition technologies, such as molecular beam epitaxy (MBE), chemical vapor deposition (CVD), or physical vapor deposition (PVD), are "line-of-sight" methods that are unsuited to the deposition of high aspect ratio structures on the extreme nanoscale. Atomic layer deposition (ALD) can coat high aspect ratio surfaces but is slow and has its limitations. There is therefore an incentive to use electrodeposition, with its ability to deposit out from a conducting surface and its ability for conformal deposition, to make nanowires and nanostructures. The templated electrodeposition of nanowires was pioneered by Penner and Martin with early studies of the deposition of poly(pyrrole) into track etch membranes[7] and there is now a considerable literature on electrodeposition through > 30 nm diameter templates. [8] Again, this work has mainly focused

on aqueous electrodeposition through track etch membranes or anodic alumina templates, nevertheless it clearly illustrates some of the potential for electrodeposition. For example Schwarzacher's group have described the deposition of profiled alloys [9] and there is a wide range of electrodeposited axially hetero-structured nanowires including metallic barcodes (200 nm diameter) [10] and recently in wire CdS /Au Schottky contacts [11]. As the diameter of the pores in the template decreases the difficulty of wetting into the pores caused by the surface tension of the electrolyte and the rate of mass transport by diffusion in the stagnant solution within the high aspect ratio pores become important limitations. Supercritical fluids offer a potential route to overcome this.

Supercritical fluids (SCFs), that is fluids above their critical temperature and pressure, have properties that are quite different from those of aqueous or non-aqueous electrolyte solutions or ionic liquids. Supercritical fluids provide an alternative range of solvents whose properties can be tuned by changing temperature and pressure. They have been widely exploited in many areas of chemistry, including extractions (such as in the large scale industrial extraction of caffeine to make decaffeinated beverages), analysis, materials modification, and the development of novel synthetic methodologies [12-17]. Crucially the absence of surface tension or phase separation allows the penetration of the smallest nanopores irrespective of the chemistry of the pore wall combined with low viscosity and hence fast rates of mass transport intermediate between those of a liquid and a gas. In addition, depending on the choice of supercritical fluid they can have high chemical stability and resistance to oxidation or reduction, giving wide potential limits[18] (more than 9 V depending on the choice of electrolyte) enabling the deposition of a wide range of reactive materials and the possibility to carry out electrodeposition at elevated temperatures. Consequently, bringing together the long established advantages of electrodeposition with the use of supercritical fluids is a potentially very attractive new approach to nanomaterials deposition.

There are, however, significant technical challenges to overcome. The supercritical fluids that would be desirable to use for electrodeposition, because they are non-corrosive and have accessible critical temperatures and pressures, have low dielectric constants, typically below 10. Consequently, it can be difficult to achieve sufficient electrolyte solubility and ionic conductivity for good electrochemistry. As a result in order to maximise solubility it is necessary to work under conditions where the density of the supercritical fluid remains close to the critical density (typically around 80 to 90% of the density of the liquid). In addition, elevated pressures are required, so specialised equipment is necessary and experiments must be carried out in sealed, pressurized vessels. Nevertheless, progress has been made and the

4

electrodeposition of copper and silver nanowires has been reported from supercritical $CO_2$ containing 13% acetonitrile as a co-solvent or supercritical difluoromethane, as well as results for the electrodeposition of germanium.[19-22]

In this paper we report a significant step forward in supercritical fluid electrodeposition that opens up a general route to the deposition of a number of p-block elements (Ga, In, Ge, Sn, Sb, Bi, Se, Te) from supercritical difluoromethane and thus very significantly widens the scope of the technique. An important feature of the electrolyte and the reagents employed in this work is that the components are mutually compatible, and therefore the results we report here pave the way for developing supercritical fluid electrodeposition towards binary and ternary semiconductor materials which are of key importance in modern electronic and optical devices, and as yet unknown for SCFED.

## EXPERIMENTAL SECTION

**Reagents.** All reagents were handled under rigorously anhydrous conditions via a dry dinitrogen atmosphere and standard Schlenk and glove-box techniques. Anhydrous $[N^nBu_4]Cl$ was obtained from Sigma and used as received. Tetra-*n*-butylammonium chlorometallate salts were made by the literature methods or as described in the Supporting Information.[23,24] Difluoromethane was supplied by INEOS Fluor Ltd, UK with a purity of 99.90 wt/wt%.

**Phase Equilibrium Measurements.** The phase equilibrium of the binary mixture of $[N^nBu_4]Cl + CH_2F_2$ was studied by using a so-called synthetic approach.[25] The synthetic approach required that the equilibrium vessel was first loaded with the $[N^nBu_4]Cl + CH_2F_2$ mixture of a known composition (e.g. the mole fraction of $[N^nBu_4]Cl$). Then the phase boundary was determined by the observation of the phase transition when varying temperature, or pressure or both. The experiments were conducted in a variable-volume view cell, the detailed description of which can be found in the literature.[26]

**Electrical Conductivity Measurements.** The electrical conductivity of $[N^nBu_4]Cl$ in $scCH_2F_2$ was measured using a newly purpose-built, high-pressure apparatus. The conductivity vessel is a three-piece, stainless steel construction, consisting of a main body, a hollow screw and an electrode holder. Two pieces of platinum foil ($0.5$ cm$^2$ each) are mounted to the inner surface of a glass tube that is attached to the electrode holder. The electrode holder is sealed to the main body with a PTFE gasket. The metal connection wires for the platinum electrodes are embedded in the PEEK (polyetheretherketone) tubing and

epoxy resins, and fed through the electrode holder and the hollow screw. The conductivity vessel is immersed in an oil bath and connected to the fluid delivery unit using PEEK tubing to avoid possible current leakage to the ground. The maximum working temperature and pressure of the conductivity apparatus is 393 K and 27 MPa, respectively.

The conductivity measurements were made with a JENWAY 4510 conductivity meter. The cell constant was calibrated using the conductivity solutions of KCl after platinization of the platinum electrodes using the standard procedures. [27] At the start of the measurements, a known amount of $[N^nBu_4]Cl$ was placed at the bottom of the conductivity vessel. The vessel was then sealed and heated to a pre-set temperature (e.g. 363 K). The pressure of the system was increased stepwise by pumping $CH_2F_2$ to the vessel. At each pressure step the contents of the vessel were agitated for more than 5 min before the conductivity was recorded. The molar concentration of $[N^nBu_4]Cl$ was kept constant because no $[N^nBu_4]Cl$ had been withdrawn from the vessel during the measurements.

**Electrochemical Measurements.** Supercritical fluid electrochemical studies were performed in a stainless steel high-pressure cell, the details of which have been described in previous publications.[22,28] The dry powdered reagents and electrolyte complexes (i.e. $[N^nBu_4]_x[MCl_y]$ and $[N^nBu_4]Cl$) were transferred into the cell inside a nitrogen-purged glove box (Belle Technology). All electrolytes were prepared with $2 \times 10^{-3}$ mol dm$^{-3}$ of the $[N^nBu_4]_x[MCl_y]$ as the redox species and $50 \times 10^{-3}$ mol dm$^{-3}$ of the $[N^nBu_4]Cl$ as the supporting electrolyte, with the exception of the $[N^nBu_4][InCl_4]$ which used $0.4 \times 10^{-3}$ mol dm$^{-3}$ of the redox species. Once sealed, the cell was removed from the glove box, connected to a high-pressure rig and heated to the desired temperature using a band heater under PID (proportional-integral-derivative) control. The sc-$CH_2F_2$ was then introduced using a specialized carbon dioxide pump (PU-1580-CO$_2$, JASCO) until the desired pressure was achieved. To ensure that the solution was homogeneous, the system was stirred during pumping using a magnetic stirrer. Stirring was stopped at least 5 minutes prior to electrochemical measurements. All experiments were carried out at 17.2 MPa and 358 K.

The electrochemical experiments were performed using a three-electrode system. A platinum mesh was used as the counter electrode, and a 0.5 mm diameter platinum disk was used as a pseudo-reference electrode. Gold disks of 1.0 or 0.5 mm diameter, polished to a mirror finish with alumina paste (1.0 and 0.3 μm) on microfiber polishing cloth (Buehler), were used as the working electrodes for voltammetric characterisation of the compounds. Cyclic voltammetry measurements were recorded at potential sweep rates of 50 mV s$^{-1}$. Films were

6

electrodeposited potentiostatically onto evaporated gold slides that consisted of microscope slides with a 5 nm chromium adhesion layer and 100 nm of gold. Prior to electrochemical experiments, the gold slides were cleaned by ultrasonic agitation in isopropanol for 10 min and then dried under flowing argon. TiN electrodes were fabricated from commercial wafers of high resistivity, intrinsic silicon (<100> orientation, 380 μm thick) coated with a 300 nm layer of PVD deposited TiN followed by a 100-200 nm thick layer of PECVD deposited silicon dioxide (Si-Mat GmbH). To prepare as electrodes the wafers were protected with a 500 nm layer of MMA resist and then diced into ~7.5 mm or 10 mm squares. The protective MMA resist was removed by cleaning in acetone (2.5 min) and IPA (2.5 min). They were then etched in buffered HF for 50 s to remove the silicon dioxide capping layer. The resistance of the TiN layer was measured to be 40-45 Ω. Electrodes were contacted to PEEK sealed stainless steel feedthroughs using silver epoxy (Eccobond 60L, Hitek Electronic Materials LTD, UK). The exposed stainless steel and silver epoxy was insulated against contact with the supercritical fluid using Struers EpoFix epoxy.

**Characterization of Electrodeposited Materials.** The deposited films were investigated using scanning electron microscopy (SEM), energy dispersive X-ray (EDX) analysis, X-ray diffraction (XRD) and Raman spectroscopy as appropriate. A Jeol JSM 6500F field emission gun scanning electron microscope (FEG-SEM) equipped with an Oxford Instruments EDX detector were used for the SEM and EDX analyses, with accelerating voltage = 20 kV. XRD patterns were collected with a Rigaku Smartlab Thin Film (9 kW) diffractometer using a 0.1 mm parallel X-ray beam (Cu-K$_\alpha$) and DTex250 1D detector. Grazing incidence patterns were collected with a 1° incident angle, and symmetric (θ-2θ) scans were used to examine preferred orientation. Data collections used either 2 or 0.5 mm length limiting slit, depending on sample size. Crystallite size calculations used data from a LaB$_6$ standard previously collected under the same conditions to model the instrumental peak shape. Data were modelled using the Rigaku PDXL2 package with patterns from the JCPDS database[29].

Raman spectroscopy was performed using a Coherent MIRA-900 Ti:Sapphire laser source in CW mode set to 702 nm and filtered using a Photonetc TLS 850 laser line filter. Raman spectra were taken in a back scattering geometry using an Olympus LMPan IR 50x objective with a power density of 2 MW/μm$^2$ on the sample. Back scattered light was collected into a Princeton Instruments TriVista triple 600 nm spectrometer, configured in subtractive mode, using 900, 900 and 1800 lines/mm gratings in three stages. Spectra was measured on a Princeton Instruments, deep depleted, liquid N$_2$-cooled silicon CCD.

**RESULTS AND DISCUSSION**

In order to successfully achieve SCFED of a range of p-block elements from sc-$CH_2F_2$, suitable (mutually compatible) reagents to provide the source of the elements and a supporting electrolyte need to be identified. For the reagents, key considerations are stability (mainly to oxygen and water) and solubility under supercritical conditions ($T$ ~358 K, $p$ ~17.2 MPa) in this low dielectric medium, as well as the ease of their electrochemical reduction. Some knowledge of speciation in the SCF is also very useful. We selected tetrabutylammonium chlorometallate salts since they are easily handled powders, can be prepared in high yields and exist for a wide range of the p-block elements, thus presenting the prospect that it will be possible to extend this system to enable deposition of binary and higher semiconductors and alloys through combining precursors in the SCF electrolyte. Previously we have described a range of different supporting electrolytes suitable for use in SCFED, the key criteria being high solubility and conductivity (dissociation into ions) in the very low dielectric SCF. Since it is expected that $Cl^-$ will be liberated during reduction of the chlorometallate precursor, $[N^nBu_4]Cl$ was identified as the most suitable supporting electrolyte, minimising the different types of ions present in the electrolyte system. Prior to its application in SCFED we therefore undertook a detailed study to determine the suitability of $[N^nBu_4]Cl$ in sc-$CH_2F_2$.

**Phase Behaviour and Conductivity of $[N^nBu_4]Cl$ in sc-$CH_2F_2$.** A single, homogeneous fluid phase is the preferential condition to carry out electrodeposition in SCFs. To measure the solubility of $[N^nBu_4]Cl$ in $CH_2F_2$, the $p$-$T$ phase boundaries of 5 binary mixtures of $[N^nBu_4]Cl$ + $CH_2F_2$ have been measured at the temperatures between 293 and 373 K and pressures up to 15 MPa, see Figure 1(b). The relevant experimental data have been interpolated to $T$ = 363 K. The resulting $p$-$x$ phase diagram is shown in Figure 1(a). Clearly, when the temperature of the electrodeposition bath is 363 K, the minimum pressure required to dissolve $3.8 \times 10^{-3}$ mole fraction (equivalent to approximately 0.06 mol dm$^{-3}$ at 20 MPa and 363 K in $CH_2F_2$) is 9.6 MPa. Therefore, the conditions employed in this study for electrodeposition were selected to ensure that $[N^nBu_4]Cl$ is completely dissolved in $CH_2F_2$, see the hatched area in Figure 1(a).
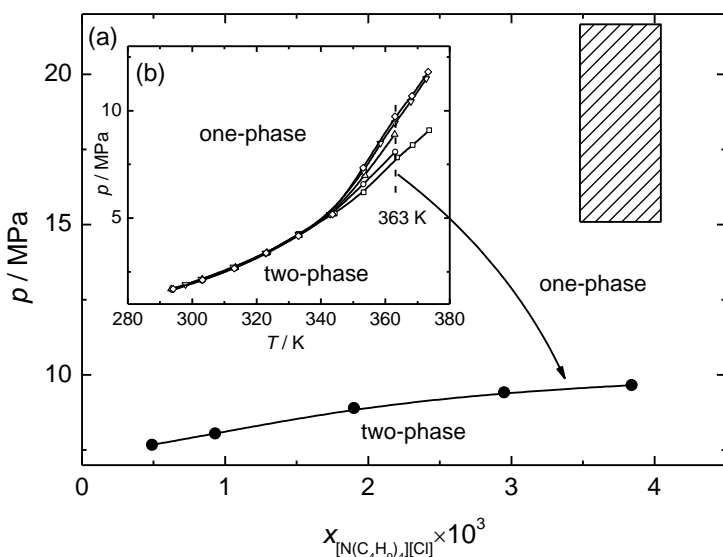
**Figure 1.** Phase diagrams of $[N^{n}Bu_4]Cl$ in $CH_2F_2$. (a) *p-x* diagram at 363 K, the hatched area represents the conditions (363 K, 15−22 MPa, and $x_{[NnBu4]Cl} = (3.5−4.0)\times10^{-3}$) used in the electrodeposition. A solution of 0.060 mol dm$^{-3}$ of $[N^{n}Bu_4]Cl$ in $CH_2F_2$ is estimated to having a mole fraction of $3.8\times10^{-3}$ at 363 K and 20 MPa. (b) *p*-T diagram for five mixtures with $x_{[NnBu4]Cl} = 0.49\times10^{-3}$ (□), $0.93\times10^{-3}$ (O), $1.90\times10^{-3}$ (△), $2.95\times10^{-3}$ (▽) and $3.84\times10^{-3}$ (◇).

Figure 2 shows the electrical conductivity of 0.060 mol dm$^{-3}$ of $[N^{n}Bu_4]Cl$ in $CH_2F_2$ at 363 K, together with the conductivity measured previously from a solution with 0.031 mol dm$^{-3}$ of $[N^{n}Bu_4][B\{3,5-C_6H_3(CF_3)_2\}_4]$ [21] which has been successfully used to electrodeposit a variety of materials in SCFs. [28] Although the molar conductivity of $[N^{n}Bu_4]Cl$ is lower than that of $[N^{n}Bu_4][B\{3,5-C_6H_3(CF_3)_2\}_4]$, it is possible to achieve the conductivity at a similar level to that of $[N^{n}Bu_4][B\{3,5-C_6H_3(CF_3)_2\}_4]$ because the high solubility of $[N^{n}Bu_4]Cl$ allows a concentrated supercritical fluid solution to be used. Furthermore, unlike $[N^{n}Bu_4][B\{3,5-C_6H_3(CF_3)_2\}_4]$, the conductivity of $[N^{n}Bu_4]Cl$ increases with pressure when the pressure is above 20 MPa, suggesting that carrying out electrodeposition above 20 MPa is also a method to improve the conductivity when using $[N^{n}Bu_4]Cl$ as a supporting electrolyte.

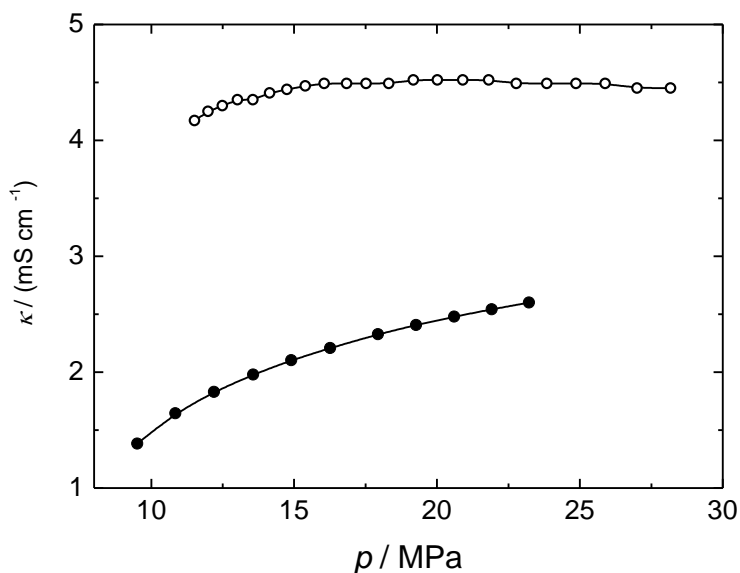**Figure 2.** Electrical conductivity of 0.060 mol dm$^{-3}$ of [N$^n$Bu$_4$]Cl (●) and 0.031 mol dm$^{-3}$ of [N$^n$Bu$_4$] [B{3,5-C$_6$H$_3$(CF$_3$)$_2$}$_4$] [21] (O) in CH$_2$F$_2$ at 363 K.


**Electrochemistry of Tetrabutylammonium Chlorometallate Salts in sc-CH$_2$F$_2$/[N$^n$Bu$_4$]Cl.**
The precursors, [N$^n$Bu$_4$][MCl$_3$] (M = Ge, Sn), [N$^n$Bu$_4$][MCl$_4$] (M = Ga, In, Sb, Bi) and
[N$^n$Bu$_4$]$_2$[MCl$_6$] (M = Se, Te) were prepared using literature methods[23,24] or slight
modifications thereof, and their identities and purity established spectroscopically (IR,
Raman, [119]Sn, [71]Ga, [115]In, ^{77}Se and [125]Te NMR) and microanalytically.

The voltammetric characteristics of all eight of the p-block elements at 17.2 MPa and 358 K
are presented in Figure 3. The grey scans included in each of the figures correspond to the
voltammetric response measured in the pure [N$^n$Bu$_4$]Cl supporting electrolyte in sc-CH$_2$F$_2$,
and establishes the potential window available in this system. The current density in the
voltammogram of the supporting electrolyte does not exceed 0.03 mA cm$^{-2}$ between −2.0 and
1.0 V, indicating that the electrolyte provides a wide potential window. Figure 3 also shows
that fluctuations are observed at cathodic potentials in the limiting current density region of
all eight voltammograms of the redox species. Fluctuations such as these often occur for
voltammetry in SCFs and it has been shown that they are due to the effects of convection in

the cell caused by temperature gradients, which are exacerbated by the low viscosity of the SCF. [30]

**Ga and In.** The voltammetry for $[N^nBu_4][GaCl_4]$ is presented in Figure 3(a). Two irreversible cathodic waves are observed at −0.50 V and −1.34 V. The magnitude of the wave heights relative to each other (i.e. 1:2) suggests that the first wave is the reduction of Ga(III) to Ga(II), while the second is the reduction of Ga(II) to Ga(0) metal. The absence of a stripping peak on the reverse anodic scan is likely due to the fact that elemental Ga is liquid at the deposition temperature of 358 K (melting point of elemental Ga = 303 K).

Figure 3(b) shows the voltammetry of the $[N^nBu_4][InCl_4]$ precursor. The current density observed for this complex is significantly smaller (approx. $^1/_{10}$) than for the other compounds. It is most likely that this is due to the lower solubility of the In(III) precursor salt in solution. Previous $^{115}$In NMR studies on a solution of $[N^nBu_4][InCl_4]$ in $CH_2Cl_2$ solution in the presence of a 10-fold excess of $[N^nBu_4]Cl$ showed that $[InCl_6]^{3-}$ is the major species present.[24] It is reasonable to assume that similar speciation occurs in sc-$CH_2F_2$, and the trianionic $[InCl_6]^{3-}$ would be expected to have much lower solubility in the low dielectric SCF. It was therefore necessary to use reduced concentrations of the $[N^nBu_4][InCl_4]$ in the plating bath to achieve satisfactory electrochemical behaviour. The voltammogram shows an irreversible reduction wave with an onset at about −0.70 V. No stripping peak is observed on the anodic scan. When the experiments were repeated in $[N^nBu_4][BF_4]$ background electrolyte the voltammetry showed a single reduction wave and stripping peak. The reduction wave was mass transport limited with an onset at about -1.10 V with a steady state current density of ~6 mA cm$^{-2}$ (see ESI). This current density is comparable to that for the other complexes in Figure 3 suggesting that in the absence of excess chloride the $[InCl_4]^-$ is soluble in the supercritical fluid.

**Ge and Sn.** The voltammogram of the $[N^nBu_4][GeCl_3]$ complex (Figure 3(c)) is characterised by a steep cathodic wave with an onset potential of approximately −1.0 V, and an erratic limiting current that extends to −1.9 V. Following the reversal of the scan direction, the current density decays to zero, indicating that the reduction of the Ge(II) to Ge(0) species is inhibited. An anodic stripping peak with an onset potential of approximately −0.50 V is also observed. There is a large discrepancy between the charge densities associated with the deposition and stripping peaks. While the total reduction charge is 1.17 mC cm$^{-2}$, the stripping charge is 0.013 mC cm$^{-2}$. This might be attributed to alloying between the deposited Ge and the gold electrode surface.

11

Figure 3(d) shows the voltammetry for $[N^nBu_4][SnCl_3]$. The voltammogram shows typical metal deposition and stripping features with a well-characterised nucleation loop and stripping peak. The onset of nucleation occurs at approximately $-1.1$ V and the stripping onset at about $-0.90$ V. The charge density associated with the deposition and stripping reactions is 0.81 mC cm$^{-2}$ and 0.58 mC cm$^{-2}$, respectively. The Faradaic efficiency is 67%.

**Sb and Bi.** The cyclic voltammetry for $[N^nBu_4][SbCl_4]$ is presented in Figure 3(e). The deposition onset of the Sb reduction is approximately $-0.32$ V. A current plateau is observed in the anodic scan until the stripping onset occurs at about $-0.42$ V. The total reduction charge for the Sb is 1.49 mC cm$^{-2}$ and the stripping charge is 0.74 mC cm$^{-2}$, with a Faradaic efficiency of 50%. The cyclic voltammetry of the $[N^nBu_4][BiCl_4]$ complex presented in Figure 3(f) shows a well-defined nucleation loop and stripping peak. The deposition onset and stripping onset are at $-0.41$ V and $-0.35$ V respectively. A small cathodic peak at $-0.31$ V observed prior to the onset of Bi reduction (see inset in Figure 3f) is attributed to the under potential deposition (UPD) of Bi. The charge associated with this peak corresponds to the adsorption of a monolayer of Bi on the surface of the gold electrode. The Faradaic efficiency of the Bi deposition is 64%, with a deposition charge of 1.85 mC cm$^{-2}$ and a stripping charge of 1.18 mC cm$^{-2}$.

**Se and Te.** The deposition voltammetry for the $[N^nBu_4]_2[SeCl_6]$ is presented in Figure 3(g). The voltammogram shows an irreversible reduction wave with an onset potential of about $-1.0$ V and a peak deposition current density at $-1.25$ V. There is a small stripping peak on the reverse anodic scan at about -0.13 V, which occurs immediately before the onset of chloride oxidation at 0.0 V.

The voltammetry of the $[N^nBu_4]_2[TeCl_6]$ is presented in Figure 3(h). This shows the typical nucleation loop and stripping peak expected for metal deposition. The deposition onset potential is approximately $-0.25$ V and the stripping onset is $-0.10$ V. The stripping peak at 0.4 V is truncated by the reversal of the anodic scan direction at 0.5 V. This is necessary as the peak becomes convoluted with chloride oxidation at potentials positive to 0.5 V. The charge associated with the Te deposition and stripping is 1.79 mC cm$^{-2}$ and 1.77 mC cm$^{-2}$, respectively, yielding a high Faradaic efficiency of 99%.

Additional voltammetry studies of the Se and Te complexes, at Pt and TiN electrodes, have shown that the onset of chloride oxidation shifts to more positive potentials for both elements on these other substrate materials (see ESI for details).
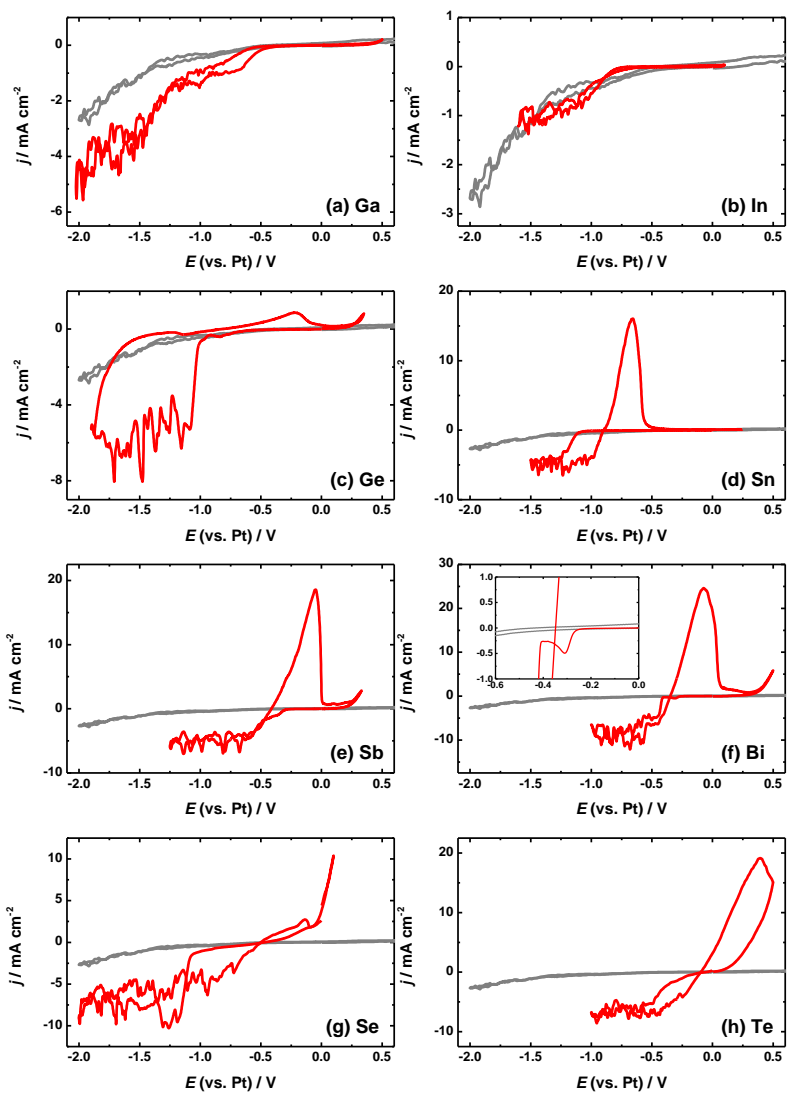
**Figure 3.** Cyclic voltammograms of (a) [N$^n$Bu$_4$][GaCl$_4$], (b) [N$^n$Bu$_4$][InCl$_4$], (c) [N$^n$Bu$_4$][GeCl$_3$], (d) [N$^n$Bu$_4$][SnCl$_3$], (e) [N$^n$Bu$_4$][SbCl$_4$], (f) [N$^n$Bu$_4$][BiCl$_4$], (g) [N$^n$Bu$_4$]$_2$[SeCl$_6$], (h) [N$^n$Bu$_4$]$_2$[TeCl$_6$] in sc-CH$_2$F$_2$ (17.2 MPa and 358 K) measured on 1.0 or 0.5 mm gold working electrodes and referenced

to a Pt pseudo-reference electrode. The concentration of the $[N^nBu_4]_x[MCl_y]$ redox species in each case was $2 \times 10^{-3}$ mol dm$^{-3}$, with the exception of the $[N^nBu_4][InCl_4]$ which used $0.4 \times 10^{-3}$ mol dm$^{-3}$. $50 \times 10^{-3}$ mol dm$^{-3}$ $[N^nBu_4]Cl$ was used as the supporting electrolyte. The potential scan rate was 50 mV s$^{-1}$. The grey scans included in each of the figures correspond to the voltammetric response measured in the pure $[N^nBu_4]Cl$ supporting electrolyte in sc-CH$_2$F$_2$.

**SCFED of p-block Elements.** The p-block elements were electrodeposited potentiostatically from sc-CH$_2$F$_2$ onto evaporated gold slide electrodes. All elements were deposited at constant potential, with the deposition potentials and times specifically selected for each element in order to obtain films of sufficient thickness for EDX and XRD analyses (1 to 2 µm), as detailed in Table 1. After depressurization, the electrodes with the deposited films were removed from the cell inside a nitrogen-purged glovebox and then gently washed by dipping into CH$_2$Cl$_2$ solution to dissolve away residual electrolyte salts. The deposited films were analysed by SEM, EDX and XRD.

**Commented [BP1]:** Pete: Is that correct?

**Table 1.** Electrodeposition parameters for all p-block elements deposited onto Au electrodes. Concentration of all precursor compounds was $2 \times 10^{-3}$ mol dm$^{-3}$, except for [InCl$_4^-$] which was $0.4 \times 10^{-3}$ mol dm$^{-3}$, with $50 \times 10^{-3}$ mol dm$^{-3}$ [TBA]Cl used as the supporting electrolyte. Pressure = 17.2 MPa, temperature = 358 K.

**Commented [BP2]:** Pete, Charlie: is that right?

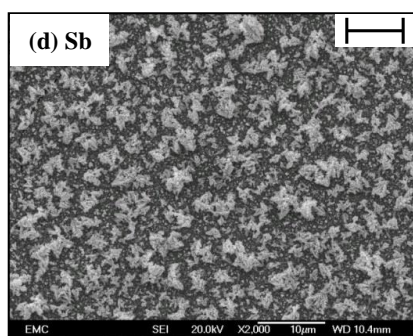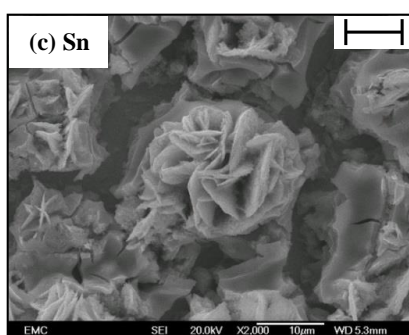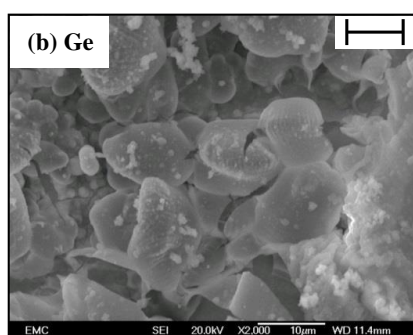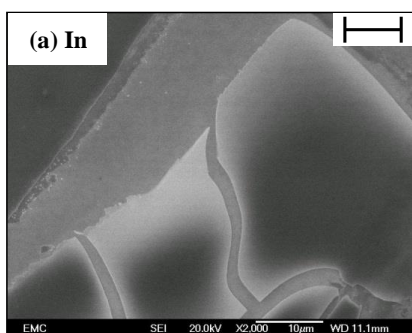| Element | Deposition potential / V *vs*. Pt | Deposition time / s | Charge passed / C |
|---|---|---|---|
| Ga | -2.00 | 5500 | 1.31 |
| In | -1.50 | 6828 | 2.65 |
| Ge | -1.80 | 5497 | 1.39 |
| Sn | -1.25 | 1001 | 1.30 |
| Sb | -0.75 | 8000 | 0.42 |
| Te | -0.80 | 3501 | 4.00 |
| Bi | -0.90 | 1034 | 1.14 |
| Se | -1.25 | 3600 | 0.64 |
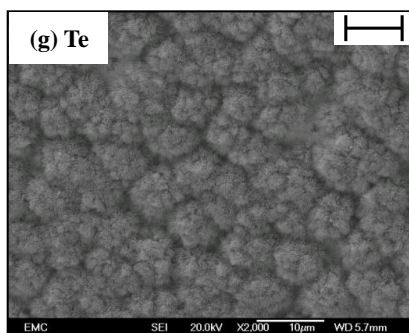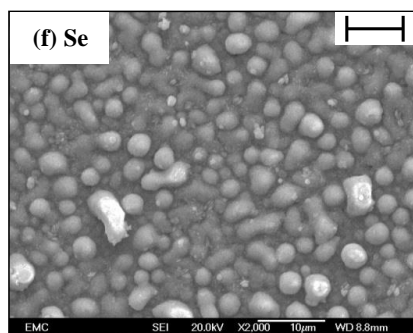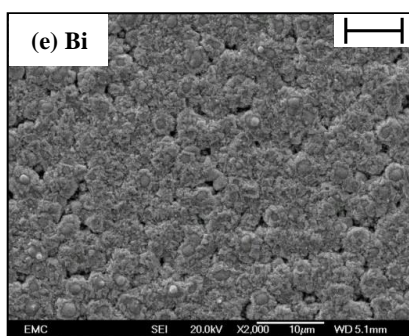
**Figure 4.** SEM images of electrodeposited films of (a) In, (b) Ge, (c) Sn, (d) Sb, (e) Bi, (f) Se and (g) Te on evaporated gold slide electrodes. The scale bars represent 10 μm. The deposition conditions are given in Table 1.

SEM images (Figure 4) show that, in general, the materials have quite uniform morphologies across the electrode surface and that the film adhesion on Au was generally good. The exceptions were the Ga which was liquid as deposited and hence the small droplets of elemental Ga readily detached from the electrode surface, and the Se which almost entirely detached from the electrode surface upon washing in the $CH_2Cl_2$ solvent. The SEM imaging shows that the Se material that remained on the electrode has a relatively smooth morphology with micro-grains of < 1 μm in length. For the Sn, Sb, Te and Bi samples, the crystalline facets are clearly visible in the images, whereas the electrodeposited In forms smoother thin layers which tend to roll up. The Ge film is also quite smooth, and shows good coverage across the electrode surface. The EDX spectra of the deposited films are shown in the ESI (Figure S2). In each case, the target element was observed as the dominant peaks, with peaks from the Au substrate also evident in some cases. In general negligible Cl was observed by EDX on samples after washing in $CH_2Cl_2$, suggesting that this procedure was highly effective.

XRD measurements were undertaken to confirm the structures of the materials electrodeposited on gold electrodes, with the exception of Ga (a liquid) and Se, where there were problems with adhesion. In the case of Sb and Te XRD provided evidence of alloying with the gold. Hence Sb, Se and Te samples were also deposited on TiN. Representative XRD patterns are presented in Figure 5, and are consistent with previously reported data for the bulk elements, except for Ge, which is amorphous as-deposited (see ESI). The experimental and literature data are presented in Table 2.
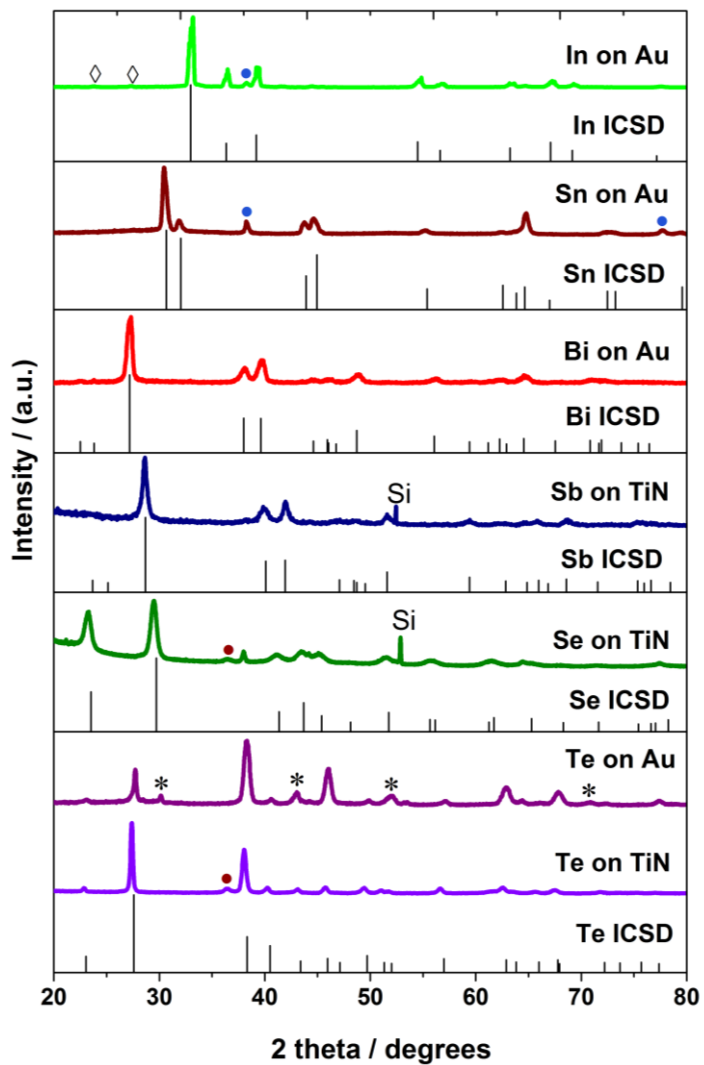
16

**Figure 5.** Grazing incidence diffraction patterns (1° incidence angle) for In, Sn, Bi, Sb, Se and Te deposited on gold and TiN. * marks the positions of peaks due to $Au_{0.3}Te_{0.7}$ alloy, and ◊ marks the positions of $AuIn2$ peaks. ● marks Au and ● marks the TiN peaks.

**Table 2.** Refined parameters from the XRD patterns in Figure 5

| Element | Crystal structure : Space group | Lattice parameters /Å | Literature lattice parameters | Crystallite size / nm |
|---|---|---|---|---|
| In | Tetragonal: I4/m m m (139) | a = 3.2411(5) c = 4.9286(9) | a = 3.2520(2) [31] c = 4.9466(2) | 22 |
| Sn | Tetragonal: I $4_1$/a m d S (141) | a = 5.8558(7) c = 3.1966(5) | a = 5.8317(2) [32] c = 3.1813(2) | 76 |
| Bi | Trigonal: R -3 m H (166) | a = 4.5394(19) c = 11.834(9) | a = 4.535(2) [33] c = 11.814(6) | 15 |
| Te | Hexagonal: P$3_1$21 (152) | a = 4.4366(15) c = 5.9040(7) | a = 4.456(1) [34] c = 5.921(2) | 38 |
| Sb on TiN | Trigonal: R -3 m H (166) | a = 4.311(3) c = 11.324(15) | a = 4.3084(2) [35] c = 11.274(6) | 56 |
| Se on TiN | Hexagonal: P$3_1$21 (152) | a = 4.389(4) c = 4.970(7) | a = 4.368(3) [36] c = 4.958(4) | 19 |
| Te on TiN | Hexagonal: P$3_1$21 (152) | a = 4.4846(11) c = 5.9568(10) | a = 4.456(1) [34] c = 5.921(2) | 39 |

The diffraction data from the electrodeposited In sample confirmed that elemental In was indeed present, although the sample was very thin, hence the diffraction pattern was dominated by peaks from the Au substrate. The pattern shown in Figure 5 was for a sample deposited from [N$^n$Bu$_4$][BF$_4$] electrolyte to improve the solubility and allow deposition of a thicker film (see ESI for details). The resultant films have no preferred orientation. Tetragonal Sn samples grown by SCFED showed elongation of the Sn 200 reflection relative to the intensity distribution from the literature XRD pattern.[32] Symmetric (θ-2θ) XRD scans confirmed some <200> preferred orientation. This is a common feature of electrodeposition processes, but in this case could also be related to the strong <111> alignment of the sputtered gold electrode surfaces. The electrodeposited antimony on gold showed the presence of Sb but also significant amounts of AuSb$_2$ (*Pa*-3, *a* = 6.63497(16) Å), the latter clearly formed by alloying with the gold electrode surface. Deposition on TiN resulted in phase pure Sb with no evidence of alloying or preferred orientation. Bi deposits showed a

normal XRD intensity distribution, consistent with polycrystalline Bi on gold. As remarked above, Se adhesion on gold was poor, however electrodeposition on TiN gave good adhesion and the resulting Se films were polycrystalline. Alloying was less significant, but still present, in Te electrodeposition on gold, with visible diffraction peaks consistent with cubic $Au_{0.3}Te_{0.7}$ ($Pm$-$3m$, $a$ = 2.9682(13) Å). The symmetric scans also showed clearly that the film had strong <001> preferred orientation due to the enhancement of the 003 reflection. Films deposited on TiN were phase pure Te with no evidence of any alignment.


## CONCLUSIONS

In this paper we have described a common approach to the electrodeposition a range of p-block elements from supercritical difluoromethane by using the chlorometallate complexes in an electrolyte of tetrabutylammonium chloride.  We have shown that under the deposition conditions, $50 \times 10^{-3}$ mol dm$^{-3}$ [N$^n$Bu$_4$]Cl at 17.2 MPa and 358 K, the system is a single, supercritical phase well away from the phase boundary and that the electrolyte has sufficient conductivity to be used for electrodeposition. The electrolyte has a stable 3 V potential window that extends to around −2.0 V $vs$. Pt. In each case, voltammetry of the complexes at gold electrodes shows clear reduction waves for deposition of the element.

Using this approach we have demonstrated the deposition of elemental Ga, In, Ge, Sn, Sb, Bi, Se, Te.  In all cases, with the exception of Ga, which is a liquid under the deposition conditions, the resulting deposits on gold or TiN were characterised by scanning electron microscopy, energy dispersive X-ray analysis, X-ray diffraction and, for Ge, Sb, Bi, Se and Te, Raman.

By using the anionic ([GaCl$_4$]$^-$, [InCl$_4$]$^-$, [GeCl$_3$]$^-$, [SnCl$_3$]$^-$, [SbCl$_4$]$^-$, and [BiCl$_4$]$^-$) and dianionic ([SeCl$_6$]$^{2-}$ and [TeCl$_6$]$^{2-}$) chlorometallates of the elements as their tetrabutylammonium salts, we demonstrate a compatible electrolyte system that can be used for these different elements. An advantage of these reagents is that they are all crystalline solids that are reasonably easy to handle and that are not highly water or oxygen sensitive.

The results presented here significantly broaden the range of materials accessible by electrodeposition from supercritical fluid and open the future possibility to deposit binary or ternary alloys and compounds of the p-block.

**ASSOCIATED CONTENT**

**Supporting Information**

Synthetic procedures for chlorometallate precursors; Raman spectra where relevant; EDX data for each element: additional voltammetry; XRD data for electrodeposited films. The Supporting Information is available free of charge on the ACS Publications website at DOI:xxxxx

## AUTHOR INFORMATION

**Corresponding Author**

*p.n.bartlett@soton.ac.uk

**Notes**

The authors declare no competing financial interest.

## ACKNOWLEDGEMENTS

## REFERENCES

(1)     Hunt, L. B. *Gold Bulletin* **1973**, *6*, 16.
(2)     Schindler, W. K., J. *Phys. Rev. B* **1997**, *55*, R1989.
(3)     Andricacos, P. C.; Uzoh, C.; Dukovic, J. O.; Horkans, J.; Deligianni, H. *IBM J. Res. & Dev.* **1998**, *42*, 567.
(4)     Cooper, E. I.; Bonhôte, C.; Heidmann, J.; Hsu, Y.; Kern, P.; Lam, J. W.; Ramasubramanian, M.; Robertson, N.; Romankiw, L. T.; Xu, H. *IBM J. Res. & Dev.* **2005**, *49*, 103.
(5)     Liu, H.; Liu, Y.; Li, J. *Phys. Chem. Chem. Phys.* **2010**, *12*, 1685.
(6)     *Electrodeposition from Ionic Liquids*

Endres, F.; MacFarlane, D.; Abbott, A., Eds.; Wiley: Chichester, 2008.
(7)     Penner, R. M.; Martin, C. R. *J. Electrochem. Soc.* **1986**, *133*.
(8)     Wu, X.-J.; Zhu, F.; Mu, C.; Liang, Y.; Xu, L.; Chen, Q.; Chen, R.; Xu, D. *Coord. Chem. Rev.* **2010** *254*, 1135.
(9)     Evans, P. R.; Yi, G.; Schwarzacher, W. *Appl. Phys. Lett.* **2000**, *76*, 481.
(10)    Nicewarner-Penã, S. R.; Freeman, R.; Reiss, B. D.; He, L.; Penã, D. J.; Walton, I. D.; Cromer, R.; Keating, C. D.; J. Natan, M. J. *Science* **2001**, *294*, 137.
(11)    Guduru, S.; Singh, V. P.; Rajaputra, S.; Mishra, S.; Mangu, R.; St. Omer, I. *Thin Solid Films* **2010**, *518* 1809.
(12)    Smith, R. D.; Wright, B. W.; Yonker, C. R. *Anal. Chem.* **1988**, *60*, 1323A.
(13)    Poliakoff, M.; Howdle, S. M.; Kazarian, S. G. *Angew. Chem., Int. Ed. Engl.* **1995**, *34*, 1275.
(14)    Cole-Hamilton, D. J. *Adv. Synth. Catal.* **2006**, *348*, 1341.

20

(15)     Licence, P.; Poliakoff, M. *NATO Sci. Ser., II,* **2008**, *246*, 171.

(16)     Johnston, K. P.; da Rocha Sandro, R. P. *J. Supercrit. Fluids* **2009**, *47*, 523.

(17)     Yang, J.; Hasell, T.; Smith, D. C.; Howdle, S. M. *J. Mater. Chem.* **2009**, *19*, 8560.

(18)     Abbott, A. P.; ardley, C. A.; Harper, J. C.; Hope, E. G. *J. Electroanal. Chem.* **1998**, *457*, 1

(19)     Ke, J.; Bartlett, P. N.; Cook, D.; Easun, T. L.; George, M. W.; Levason, W.; Reid, G.; Smith, D.; Su, W.; Zhang, W. *Phys. Chem. Chem. Phys.* **2012**, *14*, 1517.

(20)     Bartlett, P. N.; Cook, D. A.; Hector, A. L.; Levason, W.; Reid, G.; Zhang, W.; George, M. W.; Ke, J.; Smith, D. C. *Phys. Chem. Chem. Phys.* **2014**, *16*, 9202.

(21)     Bartlett, P. N.; Cook, D. C.; George, M. W.; Ke, J.; Levason, W.; Reid, G.; Su, W.; Zhang, W. *Phys. Chem. Chem. Phys.* **2011**, *13*, 190.

(22)     Ke, J.; Su, W.; Howdle, S. M.; George, M. W.; Cook, D.; Perdjon-Abel, M.; Bartlett, P. N.; Zhang, W.; Cheng, F.; Levason, W.; Reid, G.; Hyde, J.; Wilson, J.; Smith, D. C.; Mallik, K.; Sazio, P. *Proc. Natl. Acad. Sci., USA* **2009**, *106*, 14768.

(23)     Schmulbach, C. D.; Ahmed, I. Y. *Inorg. Chem.* **1971**, *10*, 1902.

(24)     Bartlett, P. N.; Cook, D.; de Groot, C. H.; Hector, A. L.; Huang, R.; Jolleys, A.; Kissling, G. P.; Levason, W.; Pearce, S. J.; Reid, G. *RSC Advances* **2013**, *3*, 15645.

(25)     Dohrn, R.; Brunner, G. *Fluid Phase Equilibria* **1995**, *106*, 213.

(26)     Licence, P.; Dellar, M. P.; Wilson, R. G. M.; Fields, P. A.; Litchfield, D.; Woods, H. M.; Poliakoff, M.; Howdle, S. M. *Rev. of Sci. Instrum.* **2004**, *75*, 3233.

(27)     Feltham, A. M.; Spiro, M. *Chem. Rev.* **1971**, *71*, 177.

(28)     Cook, D.; Bartlett, P. N.; Zhang, W.; Levason, W.; Reid, G.; Ke, J.; Su, W.; George, M. W.; Wilson, J.; Smith, D.; Mallik, K.; Barrett, E.; Sazio, P. *Phys. Chem. Chem. Phys.* **2010**, *12*, 11744.

(29)     *PDF-2 Powder Diffraction File, 2004 release*; International Center for Diffraction Data: Swarthmore, PA.

(30)     Branch, J. A.; Cook, D. A.; Bartlett, P. N. *Phys. Chem. Chem. Phys.* **2015**, *17*, 261.

(31)     Wolcyrz, M.; Kubiak, R.; Maciejewski, S. *Phys. Stat. Solidi. B - Basic Sol. St. Phys.* **1981**, *107*, 245.

(32)     Lee, J. A.; Raynor, G. V. *Proc. Phys. Soc. London* **1954**, *67*, 737.

(33)     Cucka, P.; Barrett, C. S. *Acta Crystall.* **1962**, *15*, 865.

(34)     Adenis, C.; Langer, V.; Lindqvist, O. *Acta Crystall., Sect. C* **1989**, *45*, 941.

(35)     Barrett, C. S.; Cucka, P.; Haefner, K. *Acta Crystall.* **1963**, *16*, 451.

(36)     Keller, R.; Holzapfel, W. B.; Schulz, H. *Phys. Rev, Ser. 3: Solid State* **1977**, *16*, 4404.